



Structural Insights into TMB-1 and the Role of Residues 119 and 228 in Substrate and Inhibitor Binding

Susann Skagseth,^a Tony Christopheit,^a Sundus Akhter,^b Annette Bayer,^b Ørjan Samuelsen,^{c,d} Hanna-Kirsti S. Leiros^a

The Norwegian Structural Biology Centre (NorStruct), Department of Chemistry, Faculty of Science and Technology, UiT The Arctic University of Norway, Tromsø, Norway^a; Department of Chemistry, Faculty of Science and Technology, UiT The Arctic University of Norway, Tromsø, Norway^b; Norwegian National Advisory Unit on Detection of Antimicrobial Resistance, Department of Microbiology and Infection Control, University Hospital of North Norway, Tromsø, Norway^c; Department of Pharmacy, UiT The Arctic University of Norway, Tromsø, Norway^d

ABSTRACT Metallo- β -lactamases (MBLs) threaten the effectiveness of β -lactam antibiotics, including carbapenems, and are a concern for global public health. β -Lactam/ β -lactamase inhibitor combinations active against class A and class D carbapenemases are used, but no clinically useful MBL inhibitor is currently available. Tripoli metallo- β -lactamase-1 (TMB-1) and TMB-2 are members of MBL subclass B1a, where TMB-2 is an S228P variant of TMB-1. The role of S228P was studied by comparisons of TMB-1 and TMB-2, and E119 was investigated through the construction of site-directed mutants of TMB-1, E119Q, E119S, and E119A (E119Q/S/A). All TMB variants were characterized through enzyme kinetic studies. Thermostability and crystallization analyses of TMB-1 were performed. Thiol-based inhibitors were investigated by determining the 50% inhibitory concentrations (IC_{50}) and binding using surface plasmon resonance (SPR) for analysis of TMB-1. Thermostability measurements found TMB-1 to be stabilized by high NaCl concentrations. Steady-state enzyme kinetics analyses found substitutions of E119, in particular, substitutions associated with the penicillins, to affect hydrolysis to some extent. TMB-2 with S228P showed slightly reduced catalytic efficiency compared to TMB-1. The IC_{50} levels of the new thiol-based inhibitors were 0.66 μ M (inhibitor 2a) and 0.62 μ M (inhibitor 2b), and the equilibrium dissociation constant (K_D) of inhibitor 2a was 1.6 μ M; thus, both were more potent inhibitors than L-captopril ($IC_{50} = 47 \mu$ M; $K_D = 25 \mu$ M). The crystal structure of TMB-1 was resolved to 1.75 Å. Modeling of inhibitor 2b in the TMB-1 active site suggested that the presence of the W64 residue results in T-shaped π - π stacking and R224 cation- π interactions with the phenyl ring of the inhibitor. In sum, the results suggest that residues 119 and 228 affect the catalytic efficiency of TMB-1 and that inhibitors 2a and 2b are more potent inhibitors for TMB-1 than L-captopril.

KEYWORDS metallo- β -lactamase, TMB-1, TMB-2, thermal stability, enzyme kinetics, crystal structure, mutants

Carbapenems are considered the “last resort” therapy for treating serious bacterial infections (1). The dominant mechanisms of resistance against carbapenems are β -lactamase enzymes with activity against carbapenems (also called carbapenemases) (2). Carbapenemases have been identified among Ambler class A, B, and D β -lactamases. Class B represents the metallo- β -lactamases (MBLs), which contain one or two zinc ions in the active site essential for the enzymatic activity (3). MBLs are divided into four subclasses, according to their primary structural and molecular characteristics:

Received 9 December 2016 Returned for modification 23 January 2017 Accepted 18 May 2017

Accepted manuscript posted online 30 May 2017

Citation Skagseth S, Christopheit T, Akhter S, Bayer A, Samuelsen O, Leiros HK. 2017. Structural insights into TMB-1 and the role of residues 119 and 228 in substrate and inhibitor binding. *Antimicrob Agents Chemother* 61:e02602-16. <https://doi.org/10.1128/AAC.02602-16>.

Copyright © 2017 American Society for Microbiology. All Rights Reserved.

Address correspondence to Hanna-Kirsti S. Leiros, hanna-kirsti.leiros@uit.no.

B1a (e.g., VIM, IMP, DIM, and GIM), B1b (NDM), B2 (e.g., CphA), and B3 (e.g., L1 and AIM) (4). MBLs have been found in many clinically relevant Gram-negative bacterial species such as *Pseudomonas aeruginosa*, *Acinetobacter baumannii*, and different *Enterobacteriaceae*. The dissemination of carbapenemases is a major public health problem, and there has been no effective MBL inhibitor available to date that could restore the effect of β -lactams when coadministered. Fragment-based library screening has shown that fragments containing a thiol group are able to inhibit MBLs (5). Thiol fragments are thought to inhibit MBLs through bridging the two zinc ions in the active site, by replacing the bridging hydroxyl ion (6). Studies of different thiol-containing compounds (6–11) have shown inhibitory effects on many MBLs. For instance, captopril, which has a thiol group and is used as an angiotensin converting enzyme (ACE) inhibitor for treating hypertension, shows an inhibitory effect on MBLs (12, 13).

The Tripoli metallo- β -lactamase-1 (TMB-1) gene was first discovered in a *Achromobacter xylosoxidans* strain obtained from an environmental sample in a hospital in Tripoli, Libya, in 2011 (14). TMB-1 belongs to subclass B1a and is most closely related to DIM-1 (62%) and GIM-1 (51%) at the amino acid sequence level and shows more limited similarity to IMP-1 (48%), VIM-2 (31%), and NDM-1 (29%) (14). After the initial report, TMB-1 has been identified in clinical isolates of *Acinetobacter* spp. in Japan (15), and the new TMB-1 variant named TMB-2, with the single mutation S228P, was isolated from a different hospital in Japan also in clinical isolates of *Acinetobacter* spp. (16).

The B1 MBLs contain a conserved H₁₁₆XH₁₁₈XD₁₂₀ motif (according to the standard numbering scheme for class B β -lactamases [17, 61]) that is involved in binding of both Zn1 and Zn2 in the active site. In TMB-1, serine (S) and glutamic acid (E) are located at positions 117 and 119, respectively, similarly to other MBLs, e.g., GIM-1 (18). IMP-1 and NDM-1 have serine and glutamine (Q), respectively, at position 119 (14). Studies on the effect of substitutions of second-shell-sphere residue 119 are limited. However, the residue is thought to affect the substrate specificity. Mutational studies of residue 119 have to our knowledge been reported in NDM-1 only, where glutamine was mutated to aspartic acid (D), serine, and alanine (A) (19). The MIC for NDM-1 Q119D/S/A mutants were reduced for ampicillin, meropenem, and cefepime substrates, while mutant NDM-1 Q119D showed reduced drug MIC with all substrates tested compared to NDM-1. The NDM-1 Q119D mutant showed lower levels of catalytic efficiency toward ampicillin, meropenem, ertapenem, and cefepime substrates tested in the enzyme kinetic assay than seen with NDM-1 (19). Further, residue 119 has been reported to be involved in binding of inhibitors in IMP-1, BlaB, and CphA (5, 7, 20, 21), biapenem in CphA (22) and penicillin substrates in NDM-1 (23, 24). The effect of substitutions of E119 in TMB-1 was studied here.

TMB-2 differs from TMB-1 by only the presence of a proline (P) at position 228 instead of a serine. Previous studies found that substitutions of residue 228 affected catalytic efficiency in, e.g., GIM-1 (25). Residue 228 has been thoroughly studied in several MBL enzymes; however, a proline variant similar to that found in TMB-2 has been described only in a VIM-2 R228P mutant (11). Residue 228 is located in MBL loop L3 (residues 223 to 240) and has been reported to contribute to substrate specificity (25, 26) and to be involved in inhibitor binding (8, 27).

In this study, the effects of residue 119 in the TMB-1 mutants E119Q, E119S, and E119A (E119Q/S/A) and of proline at position 228 (as in TMB-2) on the hydrolysis of a range of substrates were investigated. Mutations at position 119 were based mainly on residues found in other MBLs. Glutamic acid (E) was mutated to glutamine (Q), as in NDM-1, and to serine (S), as in IMP-1. The alanine (A) mutation was included to investigate the effect of a smaller residue at position 119. The structure of TMB-1 was solved by X-ray crystallography, and an inhibitor was modeled into the TMB-1 active site to investigate the possible modes of inhibitor binding in TMB-1. The results show that the introduction of E119Q/S/A in TMB-1 or of a S228P mutation in TMB-2 gives, in general, a reduced level of catalytic efficiency compared to TMB-1, meaning that residues 119 and 228 are important for the substrate specificity of TMB-1. The inhibitor testing shows promising results for further inhibitor optimization.

RESULTS AND DISCUSSION

Buffer optimization using thermofluor stability measurement. TMB-1, TMB-2, and the three TMB-1 mutants were expressed and purified; however, shortly after purification, the enzymes precipitated. In order to investigate buffer components with a stabilizing effect on the enzyme and to prevent precipitation, a thermofluor-based thermostability buffer was used and additive screening was performed for TMB-1 (see Table S1 in the supplemental material). The measurements revealed that increasing the NaCl concentration to 1.0 M gave a stabilization effect with a 2.4°C-higher melting temperature (T_m) for TMB-1 (see Fig. S1 in supplemental material). Consequently, 1.0 M NaCl was included in the resuspension, purification, and storage buffers. The solubility and long-term storage of TMB-1 and TMB-2 and all of the TMB-1 mutants (E119Q/S/A) were improved. The reason for the improved stability at high levels of salt could be that the TMB-1 sequence was more polar (lower hydropathicity index; Table S2) than the more neutral VIM-1 and NDM-1 sequences. The levels of purity of TMB-1, TMB-2, and the E119Q/S/A TMB-1 mutants were estimated to be >95% (Fig. S2), and the identities of TMB-1 and TMB-2 were confirmed by tandem mass spectrometry (MS/MS) analysis (data not shown).

Enzymatic kinetic characterization of TMB-1. The hydrolytic spectrum recorded for TMB-1 (Table 1) shows that the catalytic efficiency toward β -lactam substrates without a positively charged R2 group (cefoxitin, cefotaxime, meropenem, doripenem) was more efficient than for the substrates within the respective β -lactam groups containing a positively charged R2 group (cefepime, ceftazidime, and imipenem). The levels of catalytic efficiency (k_{cat}/K_m) of TMB-1 against carbapenem substrates meropenem and doripenem were 2 and 23 times higher than against the positively charged imipenem, respectively. For the cephalosporin group, the levels of catalytic efficiency of cefotaxime and cefoxitin were 3.8 and 4.4 times higher than that of ceftazidime, respectively, and 114 and 100 times higher than that of cefepime, respectively. This might have been due to the presence of the positively charged R224 in the R2 binding site of TMB-1. Most MBLs contain a positively charged K224 residue, shown to be involved in substrate binding in NDM-1 (23, 24, 28) and in inhibitor binding in NDM-1 (29) and IMP-1 (6, 30, 31). The TMB-1 hydrolysis of ampicillin, benzylpenicillin, and piperacillin substrates resulted in activity within the same range, from 0.8 to 1.3 s⁻¹ μ M⁻¹. The turnover number (k_{cat}) of ampicillin in TMB-1 is slightly better than that seen with benzylpenicillin and piperacillin, possibly due to the presence of an amine in the R1 part of ampicillin.

The hydrolytic spectrum of TMB-1 compared to those of VIM-2 (32, 33), NDM-1 (19, 34), and GIM-1 (25, 35) reveals that, in general, the catalytic efficiency for TMB-1 is lower than for VIM-2 and NDM-1, while TMB-1 shows activity similar to or somewhat higher than that of GIM-1 against the tested substrates. VIM-2 and NDM-1 hydrolyze carbapenem substrates more efficiently than TMB-1 and GIM-1; VIM-2 also shows higher catalytic efficiency toward cephalosporins than TMB-1, while TMB-1 has slightly higher activity toward cephalosporins than NDM-1. The activity of VIM-2 against benzylpenicillin is four times higher than that of TMB-1, while the catalytic efficiency of NDM-1 toward ampicillin is two times higher than that for TMB-1. The reduced activity of both TMB-1 and GIM-1 may be attributable to the presence of the tyrosine at position 233, which cannot form the interaction to substrates seen in NDM-1 MBL containing an asparagine (N) at this position. The asparagines at the 233 position, present in most MBLs, are interacting through the amine side chain with the substrate carboxyl group (28).

The role of residue 228 in enzymatic activity. Kinetic analyses of TMB-1 and TMB-2 were conducted in order to characterize the influence of the proline residue at position 228 in TMB-2 on its enzymatic properties (Table 1).

The kinetics data of TMB-2 and TMB-1 (Table 1) show a slight reduction in catalytic efficiency for TMB-2 toward all substrates used in this study and reduced activity with ampicillin as the substrate due to binding that was 3.7 times weaker. For TMB-2, tighter

TABLE 1 Steady-state enzyme kinetics of TMB-1, TMB-2, and TMB-1 mutants

Compound ^a	TMB-1			TMB-2			TMB-1 E119Q			TMB-1 E119S			TMB-1 E119A		
	K_m (μM)	k_{cat} (s^{-1})	k_{cat}/K_m ($\text{s}^{-1}/\mu\text{M}$)	K_m (μM)	k_{cat} (s^{-1})	k_{cat}/K_m ($\text{s}^{-1}/\mu\text{M}$)	K_m (μM)	k_{cat} (s^{-1})	k_{cat}/K_m ($\text{s}^{-1}/\mu\text{M}$)	K_m (μM)	k_{cat} (s^{-1})	k_{cat}/K_m ($\text{s}^{-1}/\mu\text{M}$)	K_m (μM)	k_{cat} (s^{-1})	k_{cat}/K_m ($\text{s}^{-1}/\mu\text{M}$)
Penicillins															
Benzylpenicillin	88 ± 20	78 ± 4	0.9	93 ± 19	67 ± 4	0.7	242 ± 35	33 ± 2	0.1	228 ± 40	59 ± 5	0.3	176 ± 50	146 ± 12	0.8
Ampicillin	71 ± 13	95 ± 4	1.3	263 ± 26	68 ± 2	0.3	103 ± 20	58 ± 3	0.6	102 ± 15	83 ± 3	0.8	84 ± 18	57 ± 3	0.7
Piperacillin	69 ± 14	57 ± 5	0.8	56 ± 10	34 ± 2	0.6	147 ± 29	29 ± 3	0.2	150 ± 30	69 ± 7	0.5	149 ± 23	53 ± 4	0.4
Cephalosporins															
Cefotaxime	26 ± 3	19.8 ± 0.6	0.8	15.5 ± 1.6	10.2 ± 0.3	0.7	8.9 ± 0.7	5.2 ± 0.1	0.6	15 ± 2	9.9 ± 0.3	0.7	14 ± 1	15.0 ± 0.3	1.04
Ceftazidime (R2,+)	22.4 ± 3.4	4.0 ± 0.2	0.18	17.3 ± 1.7	1.9 ± 0.05	0.1	13 ± 1	2.7 ± 0.08	0.2	13 ± 2	4.8 ± 0.2	0.37	17 ± 1	5.6 ± 0.1	0.3
Cefepime (R2,+)	194 ± 22	13.2 ± 0.6	0.07	170 ± 12	7.1 ± 0.3	0.04	124 ± 7	6.3 ± 0.2	0.05	139 ± 11	16.2 ± 0.7	0.1	234 ± 17	19.3 ± 0.8	0.08
Cefoxitin	12 ± 2	8.2 ± 0.3	0.7	10 ± 1	4.7 ± 0.05	0.47	2.9 ± 0.5	1.06 ± 0.02	0.9	3.9 ± 0.6	2.2 ± 0.04	0.6	5.07 ± 0.95	2.9 ± 0.08	0.9
Carbapenems															
Meropenem	36 ± 3	23.8 ± 0.4	0.7	27 ± 3	13.2 ± 0.4	0.5	19 ± 2	10.3 ± 0.2	0.5	34 ± 3	27.2 ± 0.5	0.8	29 ± 3	19.1 ± 0.5	0.7
Imipenem (R2,+)	126 ± 6	43.1 ± 0.6	0.3	108 ± 6	23.4 ± 0.4	0.2	98 ± 4	14.3 ± 0.1	0.1	96 ± 7	27.6 ± 0.6	0.3	131 ± 11	30.5 ± 0.8	0.2
Doripenem	97 ± 10	671 ± 20	7	85 ± 4	385 ± 5	4.6	58 ± 3	211 ± 3	3.7	65 ± 4	413 ± 7	6.4	63 ± 3	491 ± 6	7.8

^a(R2,+)^o indicates that the substrate contained a positively charged R2 group.

binding to all carbapenem and cephalosporin substrates and to most penicillin substrates was observed; however, the low turnover numbers resulted in reduced catalytic efficiency compared to that seen with TMB-1. Ampicillin and benzylpenicillin showed slightly weaker binding to TMB-2 than to TMB-1. Both substrates have a small R1 group compared to piperacillin. Residue 228 has not been shown to be involved in the binding of penicillin substrates with small R2 groups; however, the residue seems to affect neighboring residues in the active site, including the L3 loop, which again affects the binding of penicillin substrates. Residue 228 is located adjacent to the active-site Zn²⁺ in the so-called R2 binding site (36) and is a part of the MBL L3 loop. Substitutions at position 228 have been shown to be tolerated for different substrates (37) but have also been found to affect the substrate specificity of, e.g., GIM-1 (25). S228 in VIM-26 was reported to contribute to formation of a larger active-site pocket, leaving more space for substrates with larger R2 groups compared to, e.g., VIM-2 and VIM-7 with an arginine residue at this position (38). For TMB-2, the substitution of a proline at position 228 gives conformational rigidity in the L3 loop; the loop is expected to become less flexible, and this might explain the observed small reduction in the catalytic efficiency of TMB-2.

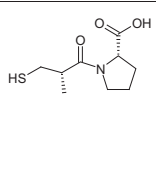
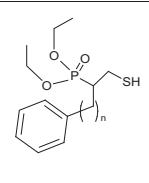
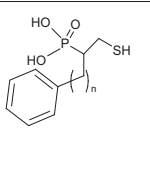
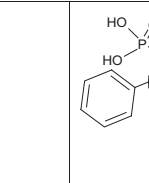
Taking the data together, the introduction of a rigid proline residue at position 228 in TMB-2 does not have a significant effect on the activity; however, there is a slight reduction in catalytic efficiency compared to TMB-1.

Effect on the enzymatic properties for the TMB-1 E119Q/S/A mutants. Our TMB-1 data show that, in general, TMB-1 has higher catalytic efficiency than the TMB-1 E119Q/S/A mutants (Table 1). The substitutions to E119Q/S/A at position 119 for TMB-1 show the most profound effect in reduced catalytic efficiency (k_{cat}/K_m) for penicillin substrates, due to both weaker binding and lower turnover of penicillin substrates, for almost all TMB-1 mutants compared to TMB-1. The effect of the TMB-1 substitutions on the catalytic activity shows that residue 119 is contributing in binding penicillin substrates. This conclusion is in agreement with reports of crystal structure complexes of NDM-1 where residue Q119 is involved in hydrogen bonding to the penicillin substrate ampicillin (23, 24). The data indicating that the TMB-1 E119Q mutant showed a reduced catalytic effect compared to wild-type TMB-1 are in contrast to the reported results for NDM-1, where NDM-1 (with Q119) had higher catalytic efficiency than NDM-1 Q119D (19). For TMB-1, the presence of a long-chained negatively charged glutamic acid at position 119 seems to increase the activity. However, the amino acid sequence identity between TMB-1 and NDM-1 is only 29%; thus, other residues nearby might contribute to this difference.

Additional residues involved in binding of ampicillin and benzylpenicillin in NDM-1 are K224 and N233 (23, 24). TMB-1 has an arginine at the 224 position and a tyrosine at the 233 position. Substitution of K224 with an arginine has been studied in NDM-1, with results showing no effect on the drug MIC for the NDM-1 K224R mutant, and the product was suggested to be able to retain the hydrogen bond to the ampicillin and other substrates (19). This supports the idea that R224 in TMB-1 contributes to the substrate binding. Substitution of Y233 to asparagine has been investigated in GIM-1, which shares 51% sequence identity with TMB-1. Here, the kinetic parameters revealed that binding of ampicillin to GIM-1 Y233N was better than that to GIM-1 Y233; however, the turnover number was lower, resulting in lower catalytic efficiency for the GIM-1 Y233N mutant (25).

Our TMB-1 kinetic studies found the binding affinity for TMB-1 E119Q toward meropenem to be about 2-fold better (lower K_m) than that for TMB-1. However, due to the low turnover (k_{cat}) for the TMB-1 E119Q mutant, the levels of catalytic efficiency were similar. Generally, TMB-1 E119Q showed the best binding to carbapenem substrates. The exception was TMB-1 E119S, which bound imipenem strongly at a level similar to that seen with TMB-1 E119Q, but the reaction rate was lower, resulting in activity in the same range as that seen with TMB-1. In crystal structures of NDM-1 with hydrolyzed meropenem (Protein Data Bank [PDB] ID [4EYL](#)), residue Q119 (named Q123

TABLE 2 Structures and IC₅₀ values of inhibitors tested with TMB-1

									
Compound	L-captopril	2a ¹	2b ¹	3a	3b	3c	10a	10b	10c
n =		2	3	2	3	4	2	3	4
IC ₅₀ (μM)	47.1	0.66	0.62	15.1	22.8	18.3	10.4	17.5	14.6
pIC ₅₀ (M)	4.33 ± 0.05	6.19 ± 0.02	6.21 ± 0.05	4.82 ± 0.03	4.64 ± 0.02	4.74 ± 0.02	4.98 ± 0.02	4.76 ± 0.03	4.84 ± 0.02

¹ Starting concentration at 250 μM, whereas other inhibitors started at 2.5 mM.

in the structure) makes a water-mediated hydrogen bond to the R1 hydroxymethyl group in meropenem (24). A similar H-bonding pattern may explain the increased binding affinity for carbapenems in TMB-1 E119Q.

Overall, the levels of catalytic efficiency of TMB-2 and TMB-1 E119Q/S/A mutants are slightly reduced compared to those seen with TMB-1, with some exceptions. The E119 and S228 residues are second-shell binding residues supporting the active site and are used to facilitate binding of β-lactam substrates. Position 119 has shown to be essential for hydrolysis of penicillin substrates but not of the other substrates.

Determination of the inhibitory activity of new thiol-based compounds. Thiol-based inhibitors have previously been tested for their inhibition potential against the MBLs VIM-2 and NDM-1 (8–10, 39) and have been shown in several studies to be good MBL inhibitors (see, e.g., references 7 and 31). In this study, eight new thiol-based inhibitors synthesized by us (40) were included and compared to L-captopril. The binding affinity (K_m) value for nitrocefin in TMB-1 was determined to be 25 μM compared to 34 μM for VIM-2, 37 μM for GIM-1, and 5 μM for NDM-1 (data not shown) and thus was determined to be a suitable reporter substrate for TMB-1.

Our new thiol-based inhibitors showed half-maximal (i.e., 50%) inhibitory concentration (IC₅₀) values ranging from 0.6 to 22.8 μM toward TMB-1 (Table 2; see also Fig. S3). Inhibitors 2a and 2b showed IC₅₀ values as low as 0.66 and 0.62 μM. The presence of a thiol group in combination with the diethyl phosphonate esters as described for inhibitors 2a and 2b resulted in inhibition properties better than those seen with corresponding mercapto- and thioacetate phosphonic acids 3a to 3c and 10a to 10c, respectively. This may indicate that the diethyl groups on the phosphonate esters (2a and 2b) are important for inhibitory efficiency. The difference in chain length between inhibitor 2a and 2b ($n = 2$ or 3 ; Table 2) did not change the inhibition potential, considering the low IC₅₀ values for both inhibitors.

Binding studies using SPR analysis with L-captopril and inhibitors 2a and 2b. A surface plasmon resonance (SPR)-based biosensor assay was used to determine the binding affinity (quantified as the equilibrium dissociation constant [K_D]) of the two best inhibitors for TMB-1. Different methods were used to immobilize TMB-1. Standard amine coupling and streptavidin-biotin capturing showed similar results, and both were used in the study. TMB-1 was immobilized on the SPR sensor surface, resulting in an immobilization level of around 1,200 response units (RU).

In order to ensure that the immobilized TMB-1 protein was active on the surface, interaction with meropenem and L-captopril was investigated. To study the interactions, 2-fold concentrations series of meropenem and L-captopril were injected over the surface. Although the signal intensity was low, a clear interaction with TMB-1 was observed (Fig. 1 and 2). Due to the rapid interactions, the rate constants were

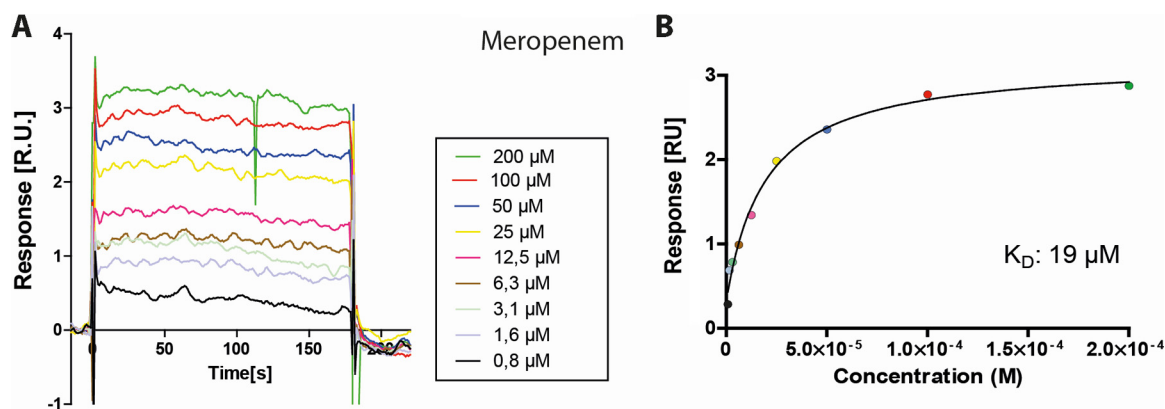


FIG 1 (A) Sensorgrams for the interaction of meropenem substrate with TMB-1, with concentrations of the substrate indicated to the right. (B) Steady-state plot for meropenem binding to TMB-1. By calculating the steady-state values from the sensorgrams, plotted as a function of the meropenem concentration and fitted to a single-binding-site model, a K_D value of 19 μM was determined.

impossible to determine. However, steady-state plots were used to calculate the binding affinity (K_D) value of meropenem of 19 μM , which is in a range similar to that of the K_m of 36 μM (Table 1) found in the steady-state kinetic measurements. The calculated binding affinity (K_D) of L-captopril was 14 μM , which was in agreement with the determined IC_{50} of 47.1 μM (Fig. 2; Table 2). The inhibition of TMB-1 with L-captopril is similar that seen with BclI and IMP-1, with IC_{50} values of 80 μM and 23 μM , respectively, while L-captopril was a better inhibitor for VIM-2 at 4 μM and a poorer inhibitor for NDM-1 at 160 μM (30). The interactions with L-captopril and meropenem showed that TMB-1 was functionally active after immobilization to the sensor surface and that the SPR assay was suitable for study of the interaction with small compounds.

Compound 2a showed a well-defined interaction with TMB-1, with clear association and dissociation phases (Fig. 2F). The sensorgrams were fitted to a 1:1 interaction model; the association constant (k_a) was $3.4 \times 10^3 \text{ M}^{-1} \text{ s}^{-1}$, and the dissociation constant (k_d) was 0.0054 s^{-1} . The K_D was calculated to be 1.6 μM , showing that compound 2a is a more potent inhibitor for TMB-1 than L-captopril (with a K_D of 14 μM).

Also, compound 2b was analyzed in a 2-fold concentration series. The obtained sensorgrams showed that compound 2b was binding to TMB-1; however, the data quality was not sufficient to determine the K_D . A possible explanation may be the racemic 50:50 mixture of the enantiomers of the inhibitor. By separating the two enantiomers, the use of the more efficient enantiomer may increase the data quality and may in addition result in better binding affinity data for both the IC_{50} and SPR measurements. This idea is supported by the data determined for the 1.55-Å structure of VIM-2_2b, where only the (R)-enantiomer fits in the observed electron density maps; thus, the enzyme had been selective (40).

Crystal structure of TMB-1. In order to get information concerning the structure-activity relationship of TMB-1, the crystal structure of the recombinant TMB-1 was solved. High-quality diffraction crystals were obtained only after buffer optimization and buffer exchange into 1.0 M NaCl in addition to 50 mM HEPES (pH 7.2) and 100 μM ZnSO_4 . The TMB-1 crystal structure was solved using molecular replacement, and a homology model was solved with the TMB-1 sequence and the DIM-1 crystal structure (PDB ID 4ZEJ). The TMB-1 crystals belong in space group $P2_12_12$, with two molecules in the asymmetric unit. The structure was resolved to 1.75 Å, and the final TMB-1 model was refined to an R -factor value of 18.9% and an R -free value of 24.9%. The mean B value was significantly lower for chain A (21.9 Å²) than for chain B (32.2 Å²), meaning that the latter corresponded to a greater number of disordered residues, which does not resemble the low Wilson B -factor value of 17.1 Å² (Table 3).

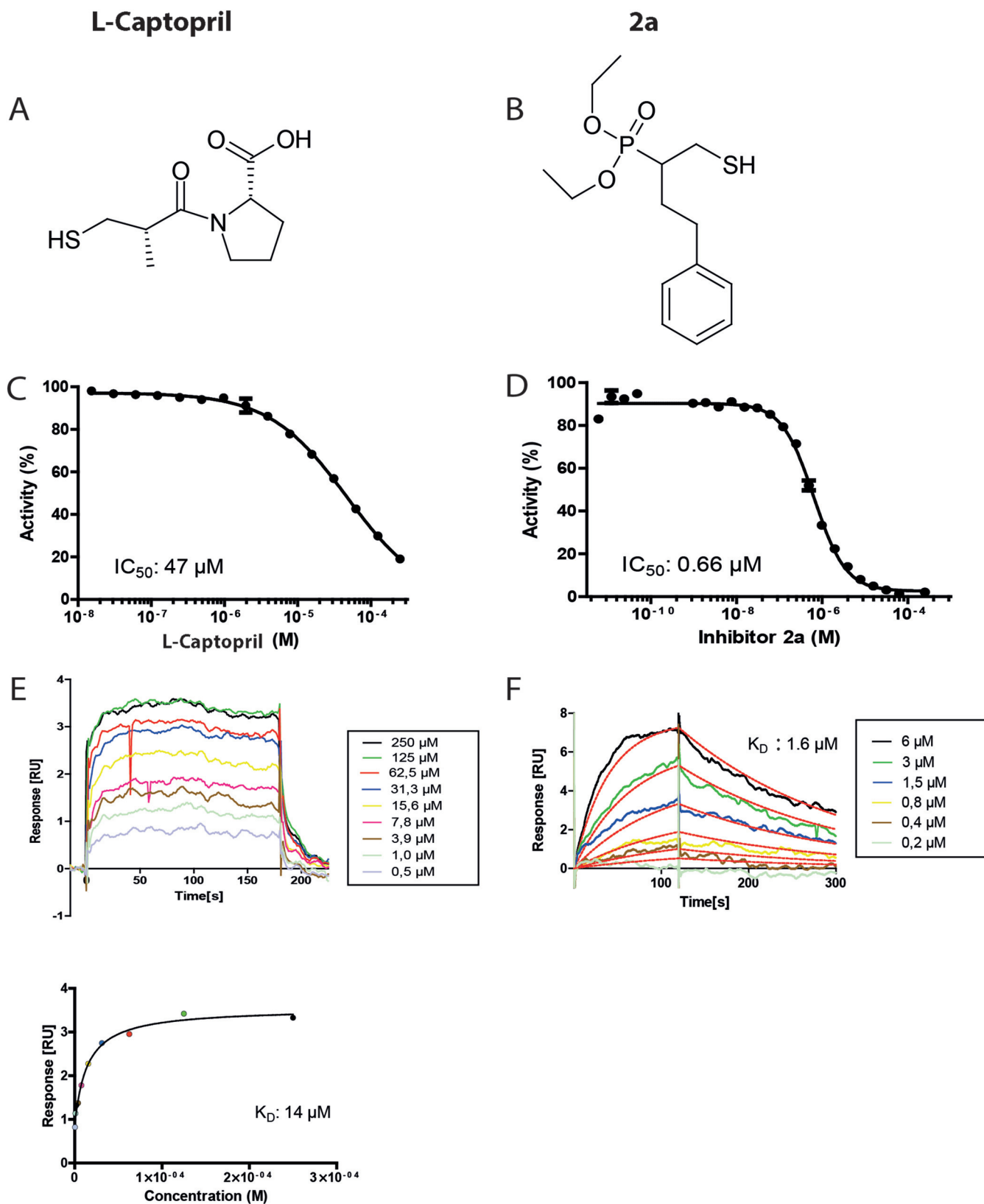


FIG 2 Structures of L-captopril (A) and inhibitor 2a (B). IC₅₀s of L-captopril (C) and inhibitor 2a (D) were calculated by fitting the data to a dose-response curve (also see Table 3). Sensorgrams for the interaction of L-captopril (E) and inhibitor 2a (F) with TMB-1, with the concentrations of the inhibitors indicated to the right. The sensorgrams for binding of inhibitor 2a to TMB-1 were fitted to a 1:1 binding model (red dotted lines). (G) Steady-state plot for binding of L-captopril to TMB-1. The K_D value was determined by calculating the steady-state values from the sensorgrams, plotted as a function of the L-captopril concentration and fitted to a single-binding-site model.

TABLE 3 X-ray data collection statistics for the TMB-1 crystal structure

Parameter	Result
Diffraction source	MX Beamline BL14.1 at BESSY II
Wavelength (Å)	0.918409
Temp (K)	100
Detector	Pilatus 6 M
Crystal-detector distance (mm)	426.55
Exposure time per image (s)	0.2
Rotation range per image (°)	0.1
Total rotation range (°)	110
Space group	P2 ₁ -2 ₁ -2
<i>a</i> , <i>b</i> , <i>c</i> (Å)	44.27, 71.40, 127.20
Resolution (Å)	47.49–1.75 (1.81–1.75)
No. of unique reflections	38,067 (2,395)
Multiplicity	3.8 (2.8)
Completeness (%)	91.9 (59.25)
<i>R</i> _{merge} (%)	8.2 (59.3)
Mean $\langle I/\sigma(I) \rangle$	10.8 (1.7)
Overall <i>B</i> -factor from Wilson plot (Å ²)	17.09

The Ramachandran plot of TMB-1 showed values of 98.15% of the residues in the most favored region, 1.39% of the residues in allowed regions, and 0.46% of the residues in the disallowed region (Table 4). Here, residue D84 represented a Ramachandran outlier in both TMB-1 chains. D84 has been described to be an outlier in many MBLs such as VIM-7 (41), VIM-2 (8), IMP-1 (6), and SPM-1 (42) due to the strained conformation seen under conditions of participation in a conserved network of H-bonds. The strained conformation of residue D84 has been suggested to play a role in folding of MBLs (8). D84 in TMB-1 forms contacts with the main and side chains of T115; the side chain of K121, Y218, and H55; and the main chain of S114. Interactions of D84 with residues T115, Y218, and K121 are also observed in VIM MBLs (41). Additional data collection and refinement statistics are given in Tables 3 and 4.

The overall structure of TMB-1 consists of the characteristic $\alpha\beta/\beta\alpha$ -fold of the MBL superfamily, with five α helices on the outside toward the solvent and the core formed by the two β -sheets containing 5 and 7 β -strands. The active site is located at the edge

TABLE 4 Refinement statistics for the TMB-1 crystal structure

Parameter	Result
PDB code	5MMD
Final <i>R</i> _{work}	0.1892
Final <i>R</i> _{free}	0.2487
No. of non-H atoms	
All atoms	3,876
Protein	3,420
Water	448
Ions	5 Zn ²⁺ , 2 Cl ⁻
RMSD	
Bonds (Å)	0.013
Angles (°)	1.39
Avg <i>B</i> factors (Å ²)	
Protein	25.90
Solvent	34.30
Zn1/Zn2	28.50
Occupancy, Zn1 (chain A/B)	1.0/0.70 (Zn1a) and 0.30 (Zn1b)
Occupancy, Zn2 (chain A/B)	0.95/1.0
Ramachandran plot	
Most favored (%)	98.15
Allowed (%)	1.39
Disallowed (%)	0.46

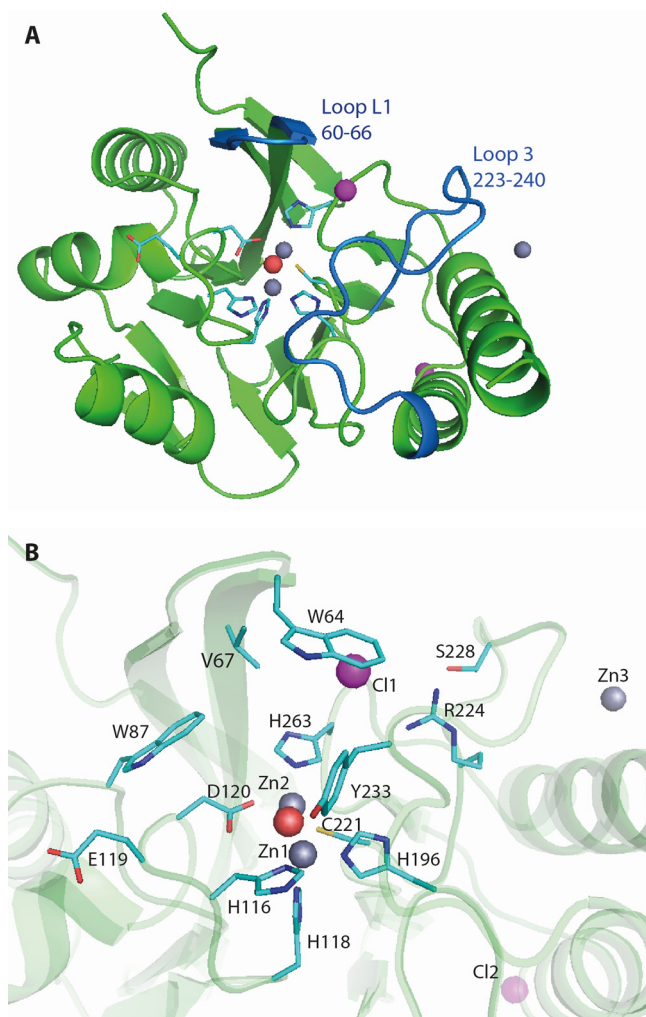


FIG 3 The overall structure of TMB-1. (A) The secondary structure of TMB-1 with active-site residues, including residue E119 (cyan), and the L1 (residues 60 to 66) and L3 (residues 223 to 240) loops (indicated in blue). (B) The TMB-1 active site, with the three zinc ions indicated in gray, the bridging water molecule indicated in red, and the two chlorine ions indicated in magenta. The residues binding Zn1 (H116, H118, and H196) and Zn2 (D120, C221, and H263) and residues V67, W64, W87, E119, R224, S228, and Y233 are described further in the paper.

of the $\beta\beta$ sandwich surrounded by two loops on each side, including residues 60 to 66 (loop L1) and residues 223 to 240 (loop L3) (Fig. 3A), which are important for the catalytic activity of the TMB-1 enzyme.

The TMB-1 active site, like those of other B1 MBLs, consists of two zinc ions: Zn1 bound to H116, H118, and H196 and Zn2 bound to D120, C221, and H263 (Fig. 3B). The zinc binding distances and the angles between the active-site residues are given in Table S3. Bridging the two zinc ions is a hydroxyl ion; during β -lactam hydrolysis, this hydroxyl ion is likely to perform the nucleophilic attack on the β -lactam carbonyl carbon (43, 44). In chain A, both zinc ions are present in a tetrahedral conformation coordinated by three binding residues and the hydroxyl ion, but in chain B, Zn1 is present in a pentahedral conformation coordinated by one additional water molecule, the hydroxyl ion, and histidine residues 116, 118, and 196. For chain A, the zinc ions were refined with full occupancy for Zn1 and an occupancy value of 0.95 for Zn2, resulting in B-factor values of 13.4 Å and 15.3 Å, respectively. In chain B, Zn1 and the H116 residue were refined with double conformations, with occupancy values of 0.70 (Zn1a) and 0.30 (Zn1b) (Table 4) and B-factor values of 18.5 Å² and 15.6 Å², respectively. The two H116 conformations for chain B were refined to occupancy values of 0.63 and 0.37.

In addition to the two Zn ions, a third Zn³ ion was observed in the TMB-1 chain A structure, bound to four water molecules and H285 in a surface exposed α -helix. Two Cl ions (Cl1/Cl2) were included in the final TMB-1 structure as interpreted from the observed electron density. Cl1 is located in between the positively charged R224 residue on the L3 loop and the W64 residue on the L1 loop, while the Cl2 ion is located between residues P254 and E255 on the surface of the structure on the other. Since the protein was crystalized from a buffer with 1.0 M NaCl, the presence of chloride ions seems likely.

Structure-activity relationship analysis of enzymatic behavior of TMB-1. In order to investigate the TMB-1 structure, a comparison of the active sites of crystal structures of NDM-1, VIM-2, and GIM-1 was performed through superposition and structure-activity relationship analysis (Fig. 4).

The results showed that the overall fold was conserved and that the TMB-1 crystal structure had a root mean square deviation (RMSD) for CA atoms of 1.31 to 1.57 Å compared to four NDM-1 crystal structures (PDB ID [4RLO](#), [4HL2](#), [3SPU](#), and [3RKJ](#)), 1.40 to 1.58 Å with five VIM-2 crystal structures (PDB ID [5LSC](#), [5MM9](#), [4C1D](#), [1KO2](#), and [4BZ3](#)), and 0.62 to 1.44 Å with four GIM-1 structures (PDB ID [2YNW](#), [2YNT](#), [2YNV](#), and [2YNU](#)). The RMSD for TMB-1 chain A compared to chain B is 0.54 Å, again showing most differences in the L1 and L3 loops. The two L1 loops of chain A and chain B are facing each other within the asymmetric unit and are thus involved in the TMB-1 crystal packing. Residues in the L3 loop are involved in substrate binding, and both the L1 and L3 loops have been shown to be flexible in, e.g., GIM-1 (18).

The active-site residues of the four compared MBLs are conserved, with some small movement of the zinc ions and bridging hydroxyl ion; however, the second-shell residues, such as residue 119 (Fig. 4a), are found in different conformations. The TMB-1 E119 residue is oriented away from the active site; however, the Q119 residue is positioned toward the active site in NDM-1 complexed with hydrolyzed cefuroxime (PDB ID [4RLO](#)). This suggests that E119 in TMB-1 may also point toward the active site upon substrate binding by a simple side chain rotation into a new rotamer. Both TMB-1 and GIM-1 have a glutamic acid residue at position 119, while VIM-2 has the shorter aspartic residue at this position (Fig. 4c). The orientation of D119 in VIM-2_2b (Fig. 4c) is shifted slightly upon inhibitor binding, while E119 in NDM-1 points inward upon cephalosporin substrate binding (Fig. 4b). The surrounding residues are not shifted significantly between the four superimposed structures, indicating that mutation at the 119 position might not have a large effect on the conformation of the active-site residues but might have a greater effect on the properties of the second-shell residues.

Further, residue R224 in TMB-1 may contribute to binding of penicillin and cephalosporins, similarly to K224 in NDM-1, which is involved in substrate binding (23, 24, 28). The tyrosine at 224 position in VIM-2 contributes to enhanced binding of positively charged substrates, such as ceftazidime and cefepime, compared to the arginine and lysine present at this position in TMB-1, NDM-1, and GIM-1, as shown for the VIM-7 H224Y mutant (36).

TMB-1 and GIM-1 both contain a tyrosine at 233 position, while most MBLs, including NDM-1 and VIM-2, contain an asparagine (45). The N233 is involved in binding of cephalosporin and penicillin substrates and in binding of inhibitors in NDM-1 (23, 24, 28) and VIM-2 (30, 46). The substitution of tyrosine to asparagine was investigated in GIM-1 and showed a reduced level of catalytic efficiency with respect to the tested substrates. However, *in silico* energy calculations of levels of ampicillin binding to GIM-1 revealed that the aromatic ring of the Y233 side chain is close to the C-6 carboxylate of hydrolyzed ampicillin β -lactam and makes a positive energy contribution to the substrate binding. Taking the data together, other surrounding second-shell residues, including Y233, might contribute to substrate and inhibitor binding, which would thus occur in a manner different from that seen with N233. Other studies on second-shell residues have found an impact on zinc binding affinity (47) and on hydrophobic interactions interfering with substrate binding (48).

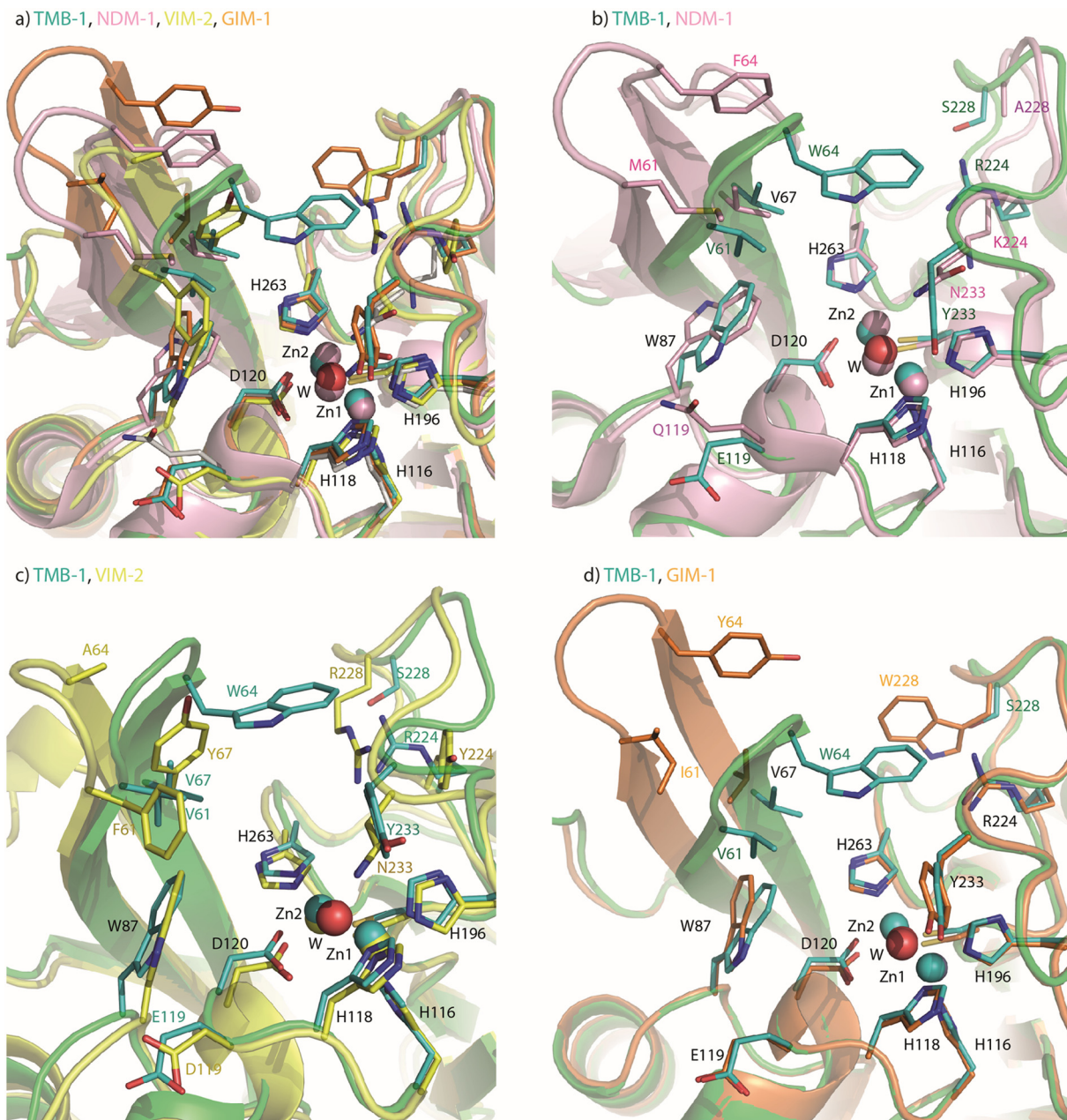


FIG 4 Comparison of the active sites of TMB-1, NDM-1, VIM-2, and GIM-2 crystal structures. (a) Superposition of crystal structures of TMB-1 (green cartoon and cyan residues), NDM-1 (light pink; PDB ID [4RL0](#)), VIM-2 (yellow; PDB ID [5MM9](#) [40]), and GIM-1 (orange; PDB ID [2YNW](#)). Residues conserved in all four structures are black. (b) Superimposed TMB-1 and NDM-1. (c) VIM-2 superimposed on TMB-1. (d) GIM-1 superposition on TMB-1. The bridging water molecule from TMB-1 is depicted in red. Residues with black labels are common for the compared structures, and different residues are labeled according to the color of the crystal structures.

One of the prominent differences in the L1 loop is the presence of W64 in TMB-1; the residue is Y64 (GIM-1), F64 (NDM-1), or A64 (VIM-2) in the other compared structures. The whole L1 loop (and W64 in particular) is found in a closed conformation in chain A of TMB-1, whereas a slightly more open active site is present in chain B. In IMP-1, W64 is involved in a T-shaped interaction with a thiophene ring of a mercarboxylate inhibitor (6), which can also be achieved in TMB-1. Residue 67 is valine in TMB-1, NDM-1, and GIM-1, while VIM-2 holds a tyrosine reported to make a π - π stacking with the phenyl ring of an inhibitor (8).

In summary, the TMB-1 active site is defined and confined by V61, W64, V67, S228, and Y233, in addition to R224, thus representing a very hydrophobic binding site

possibly contributing to the overall low level of catalytic efficiency and affecting the substrate specificity. In particular, the bulky W64 in the L1 loop restricts the size of the R2 binding site and the flexibility of the loop in TMB.

Modeling of inhibitor 2b in the TMB-1 structure. In order to investigate the interaction between TMB-1 and inhibitor 2b, the inhibitor was modeled into the active site through superposition with the previously solved 1.55-Å crystal structure of VIM-2_2b (40). The IC_{50} value of inhibitor 2b toward VIM-2 was 0.38 μM (40), which is within the same range as the IC_{50} value for TMB-1 of 0.62 μM .

The observed hydrogen bond from inhibitor 2b to N233 [$d(\text{OAE}_{\text{ligand}} \cdots \text{NE2}_{\text{N233}}) = 2.84 \text{ \AA}$] in VIM-2 cannot be present in the TMB-1 model due to the presence of Y233. However, the aromatic ring on the tyrosine may contribute to binding of the inhibitor, as seen in the free-energy calculation of GIM-1 where Y233 shows π -anion interactions with the C-7 carboxyl on hydrolyzed ampicillin (25). For TMB-1, a π interaction of Y233 with the phosphonate P = O group of 2b might explain the similar IC_{50} values of VIM-2 and TMB-1. The thiol group in inhibitor 2b can replace the bridging hydroxyl ion between the two active site zinc ions in TMB-1 as found in the VIM-2_2b structure. TMB-1 includes S228, which cannot form the cation- π interaction mediated by R228 in VIM-2_2b (PDB ID 5MM9) (Fig. 5). In TMB-1, however, R224 might contribute to the T-shaped cation- π interaction in addition to T-shaped π - π stacking from both W64 and H263. The stacking of the phenyl ring of inhibitor 2b is thus tight in binding TMB-1 but also different from that seen in VIM-2_2b (PDB ID 5MM9). The diethyl groups in the phosphonate ester of inhibitor 2b may form hydrophobic interactions with residues W87 and W64 and the carbon atoms in the E119 side chain (Fig. 5B).

The surface and L1 loop of TMB-1 is more closed than that of VIM-2 due to W64 covering the active site. The calculated electrostatic surface potential of TMB-1 and VIM-2 shows loop L1 to be negatively charged, with E62 (TMB-1) or D62 (VIM-2) pointing toward the solvent (Fig. 5). But the VIM-2 surface is more negatively charged overall, resembling the theoretic pI of 4.8 compared to 6.2 for TMB-1 (Table S2).

Conclusion. The Tripoli metallo- β -lactamase (TMB) enzymes were all found to be stabilized in buffers with high salt concentrations (1.0 M NaCl). The enzymatic characterization revealed the single S228P mutation as seen in TMB-2 to have shown a slight reduction in catalytic efficiency and four-times-reduced activity toward ampicillin compared to TMB-1. This agrees with our studies on GIM-1 showing that substitutions at position 228 affected the enzyme activity (25). In general, the catalytic performance of TMB-1 was higher than that of TMB-1 E119Q/S/A. Residue E119 was found to affect the penicillin activity, since all mutants showed catalytic efficiency levels that were 1.1 to 9 times lower. This was the case despite the fact that E119 pointed away from the active site in the new TMB-1 crystal structure resolved to 1.75 Å; thus, another side chain rotamer is likely to occur in an enzyme substrate complex.

Among the eight thiol-based inhibitors tested against TMB-1, all showed better inhibition properties than L-captopril ($IC_{50} = 47.1 \mu\text{M}$); inhibitors 2a and 2b showed the lowest IC_{50} values (0.66 μM and 0.62 μM , respectively). As demonstrated using SPR analysis and TMB-1, inhibitor 2a displayed a binding affinity (K_D) value of 1.6 μM , which was 9 times lower than for L-captopril. Modeling of binding of inhibitor 2a in TMB-1 found W64 to contribute to T-shaped π - π stacking, H263 to T-shaped stacking, and R224 to cation- π interactions with the phenyl ring of the inhibitor. Further, residues V61, W64, V67, W87, E119 (carbon chain), and Y233 formed hydrophobic interactions with the ethyl groups on the phosphonate group of the inhibitor. The aromatic Y233 can possibly make a π interaction to the P=O group of the inhibitor but not a hydrogen bond such as from N233 in VIM-2_2b. Taking the data together, the TMB-1 active site is defined and confined by residues V61, W64, V67, S228, and Y233, in addition to R224 and thus represents a very hydrophobic binding site possibly affecting substrate specificity and contributing to the overall low catalytic efficiency compared to other MBLs.

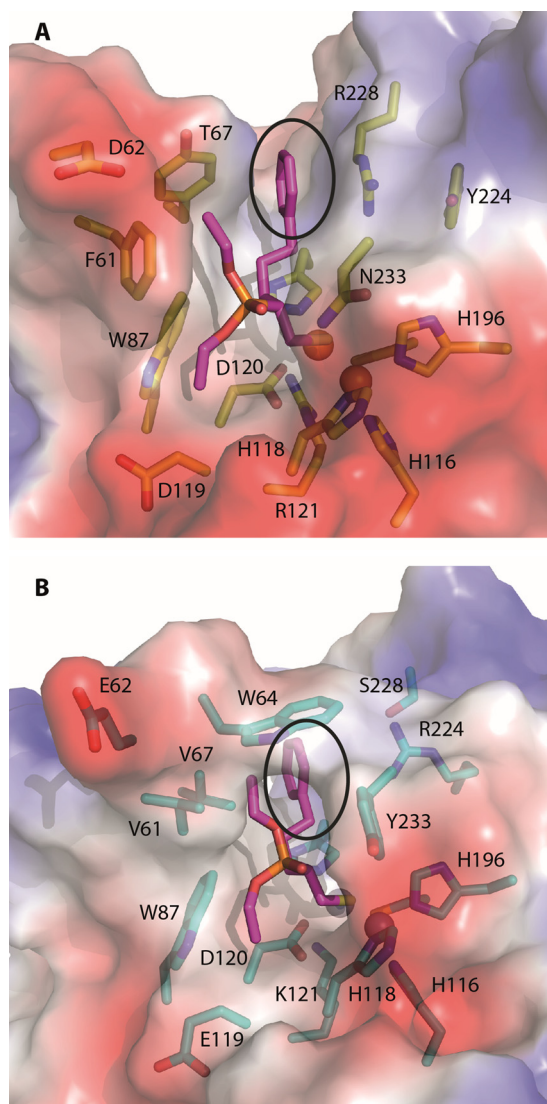


FIG 5 The active site of VIM-2 and of TMB-1 with inhibitor 2b in the active site. (A and B) Calculated electrostatic surface potential of VIM-2_2b (A) (40) and modeled inhibitor 2b (the new TMB-1; the crystal structure) (B). The two active site zinc ions are shown as spheres. The red areas represent negatively charged surface areas, and the blue areas represent positively charged surface areas. The black circles show the R2 binding site.

In a broader perspective, the TMB-1 structure, enzyme characterization, and mutation analyses presented have given further insight into the structure-activity relationship, and the presented 2a and 2b inhibitors are both good starting points for further inhibitor optimization in the fight against bacteria carrying MBLs.

MATERIALS AND METHODS

***bla*_{TMB-1} and *bla*_{TMB-2} gene constructs and site-directed mutagenesis of TMB-1.** In this study, synthetic DNA gene constructs of *bla*_{TMB-1} and *bla*_{TMB-2} in pDEST17 were codon optimized for expression in *Escherichia coli* and were purchased from Life Technologies (Thermo Fisher Scientific). The gene constructs were based on the *bla*_{TMB-1} sequence found in *Achromobacter xylosoxidans* (14) (GenBank accession number [FR771847.1](#)) and the *bla*_{TMB-2} sequence from *Acinetobacter pittii* (16) (GenBank accession number [AB758277.1](#)). Both constructs included an N-terminal hexa-His tag and a tobacco etch virus (TEV) cleavage site with amino acids ENLYFQG, followed by residues N18 to R245 for TMB-1/TMB-2, thus removing the prosegment. The gene constructs were transformed into *E. coli* BL21(DE3) pLysS (Invitrogen). TMB-1 E119Q/S/A mutants were constructed using a QuikChange site-directed mutagenesis kit (Agilent Bioscience) and the *bla*_{TMB-1} construct as the template. Primers used for the mutations are listed in Table 5. DpnI was used to digest parental DNA, and the remaining DNA was transformed into *E. coli* XL1-Blue cells (Stratagene). Luria-Bertani (LB) agar plates containing 100 μ g/ml ampicillin (Sigma-

TABLE 5 Primers used for TMB-1 site-directed mutagenesis and sequencing^a

Primer name	Forward primer sequence (5'–3')	<i>T_m</i> (°C)	Reverse primer sequence (5'–3')	<i>T_m</i> (°C)
TMB-1 E119Q	ACCCATAGCCAT <u>CAAGATA</u> AAACCGCA	74.7	TGCGGTTTTATCTT <u>GATGGCT</u> ATGGGT	74.7
TMB-1 E119S	ACCCATAGCCAT <u>TCAGATA</u> AAACCGCA	74.7	TGCGGTTTTATCT <u>GAA</u> TGGCTATGGGT	74.7
TMB-1 E119A	ACCCATAGCCAT <u>GCAGATA</u> AAACCGCA	76.2	TGCGGTTTTATCT <u>GATGGCT</u> ATGGGT	76.2
M13	GTA <u>AAACGACG</u> CCAGT	47.1	GGAAACAGCTATGACCATG	48.9

^aMutated nucleotides are underlined. Melting temperatures were calculated at http://www.biophp.org/minitools/melting_temperature/demo.php.

Aldrich) were used for selection of clones. Mutations were confirmed by DNA sequencing (BigDye Terminator cycle sequencing kit v3.1; Applied Biosystems) with the primers listed in Table 5.

Protein expression and purification. The TMB-1, TMB-2, and TMB-1 E119Q/S/A constructs were transformed into *E. coli* BL21(DE3) pLysS (Invitrogen) cells and grown as precultures in LB broth containing 100 μg/ml ampicillin and 34 μg/ml chloramphenicol (Sigma-Aldrich) at 37°C overnight. The precultures were inoculated in Terrific Broth (TB) containing 100 μg/ml ampicillin and 34 μg/ml chloramphenicol and grown to log phase (optical density at 600 nm [OD₆₀₀] of 0.5 to 1.0) at 37°C. Expression was induced using 1.0 mM (final concentration) isopropyl β-D-1-thiogalactopyranoside (IPTG; Sigma-Aldrich) and incubation at 15°C overnight with constant shaking (180 rpm). The cells were harvested using centrifugation (8,900 × *g*, 4°C, 40 min), resuspended in buffer A (50 mM HEPES [pH 7.2], 100 μM ZnSO₄, 1.0 M NaCl), and lysed by sonication. Supernatants were collected by centrifugation (25,400 × *g*, 40 min, 4°C) and used for purification of TMB-1, TMB-2, and TMB-1 mutants using a 5-ml His-Trap HP column (GE Healthcare) equilibrated with buffer A. The column was washed with 5% buffer B (50 mM HEPES [pH 7.2], 1.0 M NaCl, 100 μM ZnSO₄, 500 mM imidazole) before elution of the enzyme across a gradient of buffer B (5 to 100%) was performed. Fractions containing TMB enzymes were detected using sodium dodecyl sulfate-polyacrylamide gel electrophoresis (SDS-PAGE; Bio-Rad). An in-house-made His-tagged TEV protease (36) was added to the fractions containing TMB-1, TMB-2, or TMB-1 mutants in a 1:100 ratio of TEV protease/TMB protein to cleave off the His tag. The solutions were subsequently dialyzed at 4°C overnight in a 10-kDa-molecular-mass-cutoff SnakeSkin dialysis tube (Pierce) with buffer C (50 mM HEPES [pH 7.2], 300 mM NaCl, 100 μM ZnSO₄, 2 mM 2-mercaptoethanol). A second His-Trap purification was performed as described above to remove uncleaved TMB proteins and the His-tagged TEV protease. Fractions containing cleaved TMB enzymes were pooled and dialyzed in buffer D (50 mM Tris [pH 8.0]) before a third purification step was performed with an anion exchange Hitrap Q column and buffer E (50 mM Tris [pH 8.0], 100 μM ZnSO₄) and eluting with buffer F (50 mM Tris [pH 8.0], 100 μM ZnSO₄, 1.0 M NaCl).

The purity of the TMB-containing fractions was estimated using SDS-PAGE, and fractions with purity of above 95% were pooled and dialyzed against buffer A. The TMB proteins were concentrated by ultrafiltration using a 10-kDa-molecular-weight-cutoff Ultra centrifugal filter unit (Amicon). The yield of TMB-1 was 6.9 mg from 1 liter of culture, while the yields of TMB-2, TMB-1 E119Q, TMB-1 E119S, and TMB-1 E119A were 8.6, 3.7, 2.2, and 1.4 mg, respectively, from 1 liter of culture.

Buffer optimization using thermofluor stability measurement. Thermofluor stability measurements were performed to find stabilizing buffer components prior to crystallization. The fluorescence-based protein thermal stability was measured using a MJ Mini cyclor (Bio-Rad) over a gradient from 15 to 70°C with a heating rate of 1°C min⁻¹. The assay had a final volume of 25 μl, and the reaction mixture included 500 nM TMB-1 enzyme, 10× SYPRO Orange solution from a 5,000× stock solution (Sigma-Aldrich), and different buffer components (given in Table S1 in the supplemental material). The experiments were performed in duplicate, the results were averaged, and the melting temperature (*T_m*) values were determined from the first derivative of the inflection point of the transition. Water was used as a control, and the *T_m* values for all of the additives were higher than those calculated for water, indicated a stabilizing effect.

Determination of kinetic parameters for TMB-1, TMB-2, and TMB-1 E119Q/S/A mutants. The steady-state enzyme kinetic parameters of TMB-1 and TMB-2 and the TMB-1 variants were determined by incubation of the enzyme with different β-lactam concentrations at 25°C in buffer G (50 mM HEPES [pH 7.2], 150 mM NaCl, 100 μM ZnSO₄). The enzyme solutions were diluted to give a final concentration of 10 nM in buffer H (50 mM HEPES [pH 7.2], 150 mM NaCl, 100 μM ZnSO₄, 1 mg/ml bovine serum albumin [BSA]). BSA was added to prevent loss of enzyme activity due to a low protein concentration and to prevent protein unfolding (50, 51). The substrate concentrations ranged from 0.12 μM to 2,000 μM. All reactions were performed in UV-transparent 96-well plates or, for the penicillins, in half-well plates (Corning) with a total reaction volume of 100 μl. The initial rate of β-lactam hydrolysis was measured using a SpectraMax M2^e spectrophotometer (Molecular Devices) and fitted to the Michaelis-Menten equation (equation 1) using GraphPad Prism software (GraphPad, v5.0) to obtain the steady-state kinetic parameters *V_{max}* and *K_m* as follows:

$$v = \frac{k_{cat}[S][E]}{K_m + [S]} \quad (1)$$

where *v* is the initial velocity measured, *K_m* is the Michaelis constant, *k_{cat}* is the turnover number, and [S] and [E] are substrate and enzyme concentrations, respectively. Initial rates were measured in triplicate, and the results were averaged to determine *K_m* and *k_{cat}* values calculated from the *V_{max}* values also using the enzyme concentrations.

The indicated wavelengths and extinction coefficients were used in this study for the following antibiotics: meropenem ($\Delta_{300} = -6,500 \text{ M}^{-1} \text{ cm}^{-1}$, 0.5 to 1,000 μM), imipenem ($\Delta_{300} = -9,000 \text{ M}^{-1} \text{ cm}^{-1}$, 0.5 to 1,000 μM), doripenem ($\Delta_{300} = -7,540 \text{ M}^{-1} \text{ cm}^{-1}$, 0.5 to 1,000 μM), cefotaxime ($\Delta_{260} = -7,500 \text{ M}^{-1} \text{ cm}^{-1}$, 0.2 to 500 μM), ceftazidime ($\Delta_{260} = -9,000 \text{ M}^{-1} \text{ cm}^{-1}$, 0.1 to 250 μM), cefepime ($\Delta_{260} = -10,000 \text{ M}^{-1} \text{ cm}^{-1}$, 0.2 to 500 μM), ceftoxitin ($\Delta_{260} = -7,700 \text{ M}^{-1} \text{ cm}^{-1}$, 0.5 to 1,000 μM), benzylpenicillin ($\Delta_{235} = -775 \text{ M}^{-1} \text{ cm}^{-1}$, 1,000 to 2,000 μM), ampicillin ($\Delta_{235} = -820 \text{ M}^{-1} \text{ cm}^{-1}$, 1,000 to 2,000 μM), piperacillin ($\Delta_{235} = -820 \text{ M}^{-1} \text{ cm}^{-1}$, 0.06 to 62.5 μM), and nitrocefin ($\Delta_{282} = 17,400 \text{ M}^{-1} \text{ cm}^{-1}$, 0.5 to 250 μM).

Determination of half-maximal (50%) inhibitory concentration (IC_{50}) values for thiol-based inhibitors toward TMB-1. In our recent study, we described the organic synthesis details and inhibitor properties of many new thiol-based inhibitors against VIM-2, NDM-1, and GIM-1 (40). Here, the half-maximal (50%) inhibitory concentration (IC_{50}) values were determined for L-captopril and eight of the new thiol-based inhibitors (40) with TMB-1 at 25°C in 96-well plates using a SpectraMax M2^e spectrophotometer. The inhibitors were dissolved in dimethyl sulfoxide (DMSO) and were further diluted in buffer G, resulting in a final DMSO proportion of a maximum of 2.5% in the assay. The TMB-1 enzyme was diluted to a final concentration of 1 nM in buffer H. Nitrocefin was used at a final concentration of 50 μM as a reporter substrate. TMB-1 and the inhibitors were incubated for 5 min before nitrocefin was added and the OD_{482} was measured every 30 s for 30 min. The measurements were performed in duplicate, in an assay with a 2-fold dilution series of the inhibitors starting at 2.5 mM and 250 μM (for inhibitors 2a and 2b). The breakdown of nitrocefin was monitored at 482 nm, measuring the initial velocity for each inhibitor concentration. The values were normalized to those determined for a positive control with no inhibitor added to the measurements. The IC_{50} values were calculated by plotting the initial velocities against the inhibitor concentration and fitting the data to a dose-response curve using a constant top plateau value (100%), a constant bottom plateau value (0%), and a constant Hill slope value of 1 in the GraphPad Prism 5 software (GraphPad v5.0).

Binding studies using surface plasmon resonance (SPR). Binding of the inhibitors was studied using surface plasmon resonance (SPR)-based assays. SPR experiments were performed at 25°C using a Biacore T200 system (GE Healthcare), and the data were analyzed with Biacore T200 evaluation software 2.0 (GE Healthcare). All binding studies were performed in running buffer I (consisting of 50 mM HEPES [pH 7.2], 150 mM NaCl, 100 μM ZnSO_4 , 0.005% surfactant P-20 [GE Healthcare], and 2.5% DMSO). Standard amine coupling and streptavidin-biotin capturing were used to immobilize TMB-1 to a CM5 chip (GE Healthcare). For the standard amine coupling, TMB-1 was diluted directly in buffer J (10 mM sodium acetate [pH 5.0], 100 μM ZnSO_4) to a concentration of 200 $\mu\text{g}/\text{ml}$ and injected for 420 s over an activated surface at a flow rate of 10 $\mu\text{l}/\text{min}$. For the streptavidin-biotin capturing, TMB-1 was biotinylated in a mixture of a 1:1 molar ratio with biotinamidohexanoic acid *N*-hydroxysuccinimide ester (Sigma-Aldrich) in a 0.1 M phosphate buffer (pH 7.2) and incubated at room temperature for 30 min. An Amicon Ultra centrifugal filter (Merck Millipore Ltd.) was used with a 10-kDa-molecular-mass cutoff to remove the unreacted biotinamidohexanoic acid *N*-hydroxysuccinimide ester. Streptavidin was dissolved in 10 mM sodium acetate (pH 4.8) to a concentration of 300 $\mu\text{g}/\text{ml}$ and immobilized to the sensor surface using standard amine coupling and an injection time of 1,200 s. Biotinylated TMB-1 was injected with a 5 $\mu\text{l}/\text{min}$ flow rate for 240 s over the surface with immobilized streptavidin. A surface without immobilized TMB-1 was used for reference subtraction.

To determine the binding affinity (K_D) of meropenem, L-captopril (*N*-[(*S*)-3-mercapto-2-methylpropionyl]-L-proline; Sigma-Aldrich), and inhibitor 2a, the compounds were dissolved in running buffer I and injected in a 2-fold dilution concentration series ranging from 400 to 3 μM meropenem and from 250 to 2 μM L-captopril, while the concentration series for inhibitor 2a ranged from 6 to 0.05 μM . The association from the inhibitor was detected for 180 s or 120 s and the dissociation for 300 s. Solvent correction was used to correct bulk effects, and running buffer I was used for blank injections. All sensorgrams were subjected to reference and blank subtraction. In order to calculate the binding affinity (K_D) for meropenem and L-captopril, the steady-state values were calculated from the sensorgram and plotted as a function of concentration and fitted to a 1:1 interaction model. For inhibitor 2a, the K_D was determined by fitting the sensorgram data to a 1:1 binding model. K_D values were determined by using Biacore T200 evaluation software 2.0 (GE Healthcare).

TMB-1 and TMB-2 crystallization experiments. Crystallization trials were set up for both TMB-1 (10.4 mg/ml) and TMB-2 (11.2 mg/ml) with the sitting-drop method using a Phoenix DT crystallization robot (Rigaku) and drops of 500 nl protein and 500 nl reservoir solution in 96-well MRC plates (Molecular Dimensions) with a 60- μl reservoir volume. Crystals were achieved only for TMB-1. High-quality diffraction crystals of TMB-1 were obtained after 4 weeks of incubation at room temperature. The TMB-1 crystals were grown in 0.10 M HEPES (pH 8.0)–4.75% glycerol–32% polyethylene glycol (PEG) monomethyl ether (MME) 2000. All crystals were flash frozen in liquid nitrogen. Crystallization trials of TMB-1 were performed using low-salt buffer (<200 mM NaCl) and high-salt buffer A (1.0 M NaCl, 50 mM HEPES [pH 7.2], 100 μM ZnSO_4).

Data collection and structure determination, refinement, and analysis. The X-ray data collection was performed at beamline BL14.1 at Berliner Elektronenspeicherring-Gesellschaft für Synchrotronstrahlung mbH (BESSY), Berlin, Germany, and the data were integrated, scaled, and truncated in XDS, XSCALE (52), and AIMLESS (53).

A homology model was made using DIM-1 (PDB ID 4ZEJ) and the TMB-1 sequence in the program SWISS-MODEL (54), and this model was used to solve the TMB-1 structure by molecular replacement in PHASER crystallographic software (55). The structure was refined in Phenix software (56) with manual rebuilding in the graphical program WinCoot (57). All structural figures were made using PyMol (58).

The theoretical values for pI and the grand average of hydropathicity index (GRAVY) were calculated using the ExPasy Web server (<http://web.expasy.org/protparam/>). The residues included in the gene constructs were TMB-1 G plus N18-R245, NDM-1 G plus G29-R294 (59), VIM-2 G plus V27-E245 (27), and GIM-1 A plus G19-D250 (25), where the first residue remains after TEV cleavage. GRAVY values are calculated by adding the hydropathy value for each residue and dividing by the sequence length (60) where, e.g., isoleucine has a value of +4.5 (most hydrophobic) and arginine has a value of -4.5 (most polar).

Accession number(s). Coordinate and structure factor files for TMB-1 (PDB ID [5MMD](#)) have been deposited and released in the Protein Data Bank (PDB).

SUPPLEMENTAL MATERIAL

Supplemental material for this article may be found at <https://doi.org/10.1128/AAC.02602-16>.

SUPPLEMENTAL FILE 1, PDF file, 0.9 MB.

ACKNOWLEDGMENTS

We acknowledge Trine Josefine O. Carlsen for cloning, purification, and crystallization of proteins.

This work has been funded by the research Council of Norway (FRIMEDBIO 2011 [213808] and SYNKNOYT 2011 [218539]), and this is highly acknowledged. The provision of beam time at BL14.1 BESSY II, Berlin, Germany, is highly valued.

H.-K.S.L., S.S., T.C., and Ø.S. designed the experiments. S.S. performed biochemical and thermofluor characterization. S.A. and A.B. performed the organic synthesis experiments. S.S. and T.C. performed inhibitor binding and SPR assays. S.S. and H.-K.S.L. solved and analyzed three-dimensional (3D) structures. S.S., H.-K.S.L., T.C., and Ø.S. analyzed data and wrote the paper. All of us approved the final version of the manuscript.

REFERENCES

- Boucher HW, Talbot GH, Bradley JS, Edwards JE, Gilbert D, Rice LB, Scheld M, Spellberg B, Bartlett J. 2009. Bad bugs, no drugs: no ESCAPE! An update from the Infectious Diseases Society of America. *Clin Infect Dis* 48:1–12. <https://doi.org/10.1086/595011>.
- Pratt RF. 2016. β -Lactamases: why and how. *J Med Chem* 59:8207–8220. <https://doi.org/10.1021/acs.jmedchem.6b00448>.
- Cornaglia G, Giamarellou H, Rossolini GM. 2011. Metallo- β -lactamases: a last frontier for β -lactams? *Lancet Infect Dis* 11:381–393. [https://doi.org/10.1016/S1473-3099\(11\)70056-1](https://doi.org/10.1016/S1473-3099(11)70056-1).
- Bush K. 2013. The ABCD's of β -lactamase nomenclature. *J Infect Chemother* 19:549–559. <https://doi.org/10.1007/s10156-013-0640-7>.
- Vella P, Hussein WM, Leung EW, Clayton D, Ollis DL, Mitic N, Schenk G, McGear RP. 2011. The identification of new metallo- β -lactamase inhibitors leads from fragment-based screening. *Bioorg Med Chem Lett* 21:3282–3285. <https://doi.org/10.1016/j.bmcl.2011.04.027>.
- Concha NO, Janson CA, Rowling P, Pearson S, Cheever CA, Clarke BP, Lewis C, Galleni M, Frère JM, Payne DJ, Bateson JH, Abdel-Meguid SS. 2000. Crystal structure of the IMP-1 metallo- β -lactamase from *Pseudomonas aeruginosa* and its complex with a mercaptocarboxylate inhibitor: binding determinants of a potent, broad-spectrum inhibitor. *Biochemistry* 39:4288–4298. <https://doi.org/10.1021/bi992569m>.
- Liénard BM, Garau G, Horsfall L, Karsiotis AI, Dambon C, Lassaux P, Papamichael C, Roberts GC, Galleni M, Dideberg O, Frère JM, Schofield CJ. 2008. Structural basis for the broad-spectrum inhibition of metallo- β -lactamases by thiols. *Org Biomol Chem* 6:2282–2294. <https://doi.org/10.1039/b802311e>.
- Yamaguchi Y, Jin W, Matsunaga K, Ikemizu S, Yamagata Y, Wachino J, Shibata N, Arakawa Y, Kurosaki H. 2007. Crystallographic investigation of the inhibition mode of a VIM-2 metallo- β -lactamase from *Pseudomonas aeruginosa* by a mercaptocarboxylate inhibitor. *J Med Chem* 50:6647–6653. <https://doi.org/10.1021/jm701031n>.
- Jin W, Arakawa Y, Yasuzawa H, Taki T, Hashiguchi R, Mitsutani K, Shoga A, Yamaguchi Y, Kurosaki H, Shibata N, Ohta M, Goto M. 2004. Comparative study of the inhibition of metallo- β -lactamases (IMP-1 and VIM-2) by thiol compounds that contain a hydrophobic group. *Biol Pharm Bull* 27:851–856. <https://doi.org/10.1248/bpb.27.851>.
- Klingler FM, Wichelhaus TA, Frank D, Cuesta-Bernal J, El-Delik J, Müller HF, Sjutts H, Gottig S, Koenigs A, Pos KM, Pogoryelov D, Proschak E. 2015. Approved drugs containing thiols as inhibitors of metallo- β -lactamases: strategy to combat multidrug-resistant bacteria. *J Med Chem* 58:3626–3630. <https://doi.org/10.1021/jm501844d>.
- Mojica MF, Mahler SG, Bethel CR, Taracila MA, Kosmopoulou M, Papp-Wallace KM, Llarrull LI, Wilson BM, Marshall SH, Wallace CJ, Villegas MV, Harris ME, Vila AJ, Spencer J, Bonomo RA. 2015. Exploring the role of residue 228 in substrate and inhibitor recognition by VIM metallo- β -lactamases. *Biochemistry* 54:3183–3196. <https://doi.org/10.1021/acs.biochem.5b00106>.
- Li N, Xu Y, Xia Q, Bai C, Wang T, Wang L, He D, Xie N, Li L, Wang J, Zhou HG, Xu F, Yang C, Zhang Q, Yin Z, Guo Y, Chen Y. 2014. Simplified captopril analogues as NDM-1 inhibitors. *Bioorg Med Chem Lett* 24:386–389. <https://doi.org/10.1016/j.bmcl.2013.10.068>.
- Guo Y, Wang J, Niu G, Shui W, Sun Y, Zhou H, Zhang Y, Yang C, Lou Z, Rao Z. 2011. A structural view of the antibiotic degradation enzyme NDM-1 from a superbug. *Protein Cell* 2:384–394. <https://doi.org/10.1007/s13238-011-1055-9>.
- El Salabi A, Borra PS, Toleman MA, Samuelsen Ø, Walsh TR. 2012. Genetic and biochemical characterization of a novel metallo- β -lactamase, TMB-1, from an *Achromobacter xylosoxidans* strain isolated in Tripoli, Libya. *Antimicrob Agents Chemother* 56:2241–2245. <https://doi.org/10.1128/AAC.05640-11>.
- Kayama S, Shigemoto N, Shimizu W, Kuwahara R, Ikeda M, Ikebe K, Maeda K, Hisatsune J, Ohge H, Sugai M. 2014. Tripoli metallo- β -lactamase-1 (TMB-1)-producing *Acinetobacter* spp. with decreased resistance to imipenem in Japan. *Antimicrob Agents Chemother* 58:2477–2478. <https://doi.org/10.1128/AAC.01790-13>.
- Suzuki S, Matsui M, Suzuki M, Sugita A, Kosuge Y, Kodama N, Ichise Y, Shibayama K. 2013. Detection of tripoli metallo- β -lactamase 2 (TMB-2), a variant of bla_{TMB-1}, in clinical isolates of *Acinetobacter* spp. in Japan. *J Antimicrob Chemother* 68:1441–1442. <https://doi.org/10.1093/jac/dkt031>.
- Galleni M, Lamotte-Brasseur J, Rossolini GM, Spencer J, Dideberg O, Frère JM; Metallo- β -lactamases Working Group. 2001. Standard numbering scheme for class B β -lactamases. *Antimicrob Agents Chemother* 45:660–663. <https://doi.org/10.1128/AAC.45.3.660-663.2001>.
- Borra PS, Samuelsen Ø, Spencer J, Walsh TR, Lorentzen MS, Leiros HK. 2013. Crystal structures of *Pseudomonas aeruginosa* GIM-1: active-site plasticity in metallo- β -lactamases. *Antimicrob Agents Chemother* 57:848–854. <https://doi.org/10.1128/AAC.02227-12>.

19. Chiou J, Leung TY, Chen S. 2014. Molecular mechanisms of substrate recognition and specificity of New Delhi metallo- β -lactamase. *Antimicrob Agents Chemother* 58:5372–5378. <https://doi.org/10.1128/AAC.01977-13>.
20. Hiraawa Y, Saito J, Watanabe T, Yamada M, Morinaka A, Fukushima T, Kudo T. 2014. X-ray crystallographic analysis of IMP-1 metallo- β -lactamase complexed with a 3-aminophthalic acid derivative, structure-based drug design, and synthesis of 3,6-disubstituted phthalic acid derivative inhibitors. *Bioorg Med Chem Lett* 24:4891–4894. <https://doi.org/10.1016/j.bmcl.2014.08.039>.
21. García-Saez I, Hopkins J, Papamichael C, Franceschini N, Amicosante G, Rossolini GM, Galleni M, Frère JM, Dideberg O. 2003. The 1.5-Å structure of *Chryseobacterium meningosepticum* zinc β -lactamase in complex with the inhibitor, D-captropil. *J Biol Chem* 278:23868–23873. <https://doi.org/10.1074/jbc.M301062200>.
22. Garau G, Bebrone C, Anne C, Galleni M, Frere JM, Dideberg O. 2005. A metallo- β -lactamase enzyme in action: crystal structures of the monozinc carbapenemase CphA and its complex with biapenem. *J Mol Biol* 345:785–795. <https://doi.org/10.1016/j.jmb.2004.10.070>.
23. Zhang H, Hao Q. 2011. Crystal structure of NDM-1 reveals a common β -lactam hydrolysis mechanism. *FASEB J* 25:2574–2582. <https://doi.org/10.1096/fj.11-184036>.
24. King DT, Worrall LJ, Gruninger R, Strynadka NC. 2012. New Delhi metallo- β -lactamase: structural insights into β -lactam recognition and inhibition. *J Am Chem Soc* 134:11362–11365. <https://doi.org/10.1021/ja303579d>.
25. Skagseth S, Carlsen TJ, Bjerga GE, Spencer J, Samuelsen Ø, Leiros HK. 2016. Role of residues W228 and Y233 in the structure and activity of metallo- β -lactamase GIM-1. *Antimicrob Agents Chemother* 60:990–1002. <https://doi.org/10.1128/AAC.02017-15>.
26. Merino M, Perez-Llarena FJ, Kerff F, Poza M, Mallo S, Rumbo-Feal S, Beceiro A, Juan C, Oliver A, Bou G. 2010. Role of changes in the L3 loop of the active site in the evolution of enzymatic activity of VIM-type metallo- β -lactamases. *J Antimicrob Chemother* 65:1950–1954. <https://doi.org/10.1093/jac/dkq259>.
27. Christopheit T, Carlsen TJ, Helland R, Leiros HK. 2015. Discovery of novel inhibitor scaffolds against the metallo- β -lactamase VIM-2 by surface plasmon resonance (SPR) based fragment screening. *J Med Chem* 58:8671–8682. <https://doi.org/10.1021/acs.jmedchem.5b01289>.
28. Feng H, Ding J, Zhu D, Liu X, Xu X, Zhang Y, Zang S, Wang DC, Liu W. 2014. Structural and mechanistic insights into NDM-1 catalyzed hydrolysis of cephalosporins. *J Am Chem Soc* 136:14694–14697. <https://doi.org/10.1021/ja508388e>.
29. Christopheit T, Albert A, Leiros HK. 2016. Discovery of a novel covalent non- β -lactam inhibitor of the metallo- β -lactamase NDM-1. *Bioorg Med Chem* 24:2947–2953. <https://doi.org/10.1016/j.bmc.2016.04.064>.
30. Brem J, van Berkel SS, Zollman D, Lee SY, Gileadi O, McHugh PJ, Walsh TR, McDonough MA, Schofield CJ. 2015. Structural basis of metallo- β -lactamase inhibition by captropil stereoisomers. *Antimicrob Agents Chemother* 60:142–150. <https://doi.org/10.1128/AAC.01335-15>.
31. Hinchliffe P, Gonzalez MM, Mojica MF, Gonzalez JM, Castillo V, Saiz C, Kosmopoulou M, Tooke CL, Llarrull LI, Mahler G, Bonomo RA, Vila AJ, Spencer J. 2016. Cross-class metallo- β -lactamase inhibition by bisthiazolidines reveals multiple binding modes. *Proc Natl Acad Sci U S A* 113:E3745–E3754. <https://doi.org/10.1073/pnas.1601368113>.
32. Docquier JD, Lamotte-Brasseur J, Galleni M, Amicosante G, Frere JM, Rossolini GM. 2003. On functional and structural heterogeneity of VIM-type metallo- β -lactamases. *J Antimicrob Chemother* 51:257–266. <https://doi.org/10.1093/jac/dkg067>.
33. Borgianni L, Vandenameele J, Matagne A, Bini L, Bonomo RA, Frere JM, Rossolini GM, Docquier JD. 2010. Mutational analysis of VIM-2 reveals an essential determinant for metallo- β -lactamase stability and folding. *Antimicrob Agents Chemother* 54:3197–3204. <https://doi.org/10.1128/AAC.01336-09>.
34. Yong D, Toleman MA, Giske CG, Cho HS, Sundman K, Lee K, Walsh TR. 2009. Characterization of a new metallo- β -lactamase gene, *bla*_{NDM-11}, and a novel erythromycin esterase gene carried on a unique genetic structure in *Klebsiella pneumoniae* sequence type 14 from India. *Antimicrob Agents Chemother* 53:5046–5054. <https://doi.org/10.1128/AAC.00774-09>.
35. Castanheira M, Toleman MA, Jones RN, Schmidt FJ, Walsh TR. 2004. Molecular characterization of a β -lactamase gene, *bla*_{GIM-11}, encoding a new subclass of metallo- β -lactamase. *Antimicrob Agents Chemother* 48:4654–4661. <https://doi.org/10.1128/AAC.48.12.4654-4661.2004>.
36. Leiros HK, Skagseth S, Edvardsen KSW, Lorentzen MS, Bjerga GE, Leiros I, Samuelsen Ø. 2014. His224 alters the R2 drug binding site and Phe218 influences the catalytic efficiency of the metallo- β -lactamase VIM-7. *Antimicrob Agents Chemother* 58:4826–4836. <https://doi.org/10.1128/AAC.02735-13>.
37. Materon IC, Beharry Z, Huang W, Perez C, Palzkill T. 2004. Analysis of the context dependent sequence requirements of active-site residues in the metallo- β -lactamase IMP-1. *J Mol Biol* 344:653–663. <https://doi.org/10.1016/j.jmb.2004.09.074>.
38. Leiros HK, Edvardsen KS, Bjerga GE, Samuelsen Ø. 2015. Structural and biochemical characterization of VIM-26 shows that Leu224 has implications for the substrate specificity of VIM metallo- β -lactamases. *FEBS J* 282:1031–1042. <https://doi.org/10.1111/febs.13200>.
39. González MM, Kosmopoulou M, Mojica MF, Castillo V, Hinchliffe P, Pettinati I, Brem J, Schofield CJ, Mahler G, Bonomo RA, Llarrull LI, Spencer J, Vila AJ. 2015. Bisthiazolidines: a substrate-mimicking scaffold as an inhibitor of the NDM-1 carbapenemase. *ACS Infect Dis* 1:544–554. <https://doi.org/10.1021/acscinfed.5b00046>.
40. Skagseth S, Akhter S, Paulsen MH, Muhammad Z, Lauksund S, Samuelsen Ø, Leiros HK, Bayer A. 2017. Metallo- β -lactamase inhibitors by bioisosteric replacement: preparation, activity and binding. *Eur J Med Chem* 135:159–173. <https://doi.org/10.1016/j.ejmech.2017.04.035>.
41. Borra PS, Leiros HK, Ahmad R, Spencer J, Leiros I, Walsh TR, Sundsfjord A, Samuelsen Ø. 2011. Structural and computational investigations of VIM-7: insights into the substrate specificity of vim metallo- β -lactamases. *J Mol Biol* 411:174–189. <https://doi.org/10.1016/j.jmb.2011.05.035>.
42. Murphy TA, Catto LE, Halford SE, Hadfield AT, Minor W, Walsh TR, Spencer J. 2006. Crystal structure of *Pseudomonas aeruginosa* SPM-1 provides insights into variable zinc affinity of metallo- β -lactamases. *J Mol Biol* 357:890–903. <https://doi.org/10.1016/j.jmb.2006.01.003>.
43. Wang Z, Fast W, Benkovic SJ. 1999. On the mechanism of the metallo- β -lactamase from *Bacteroides fragilis*. *Biochemistry* 38:10013–10023. <https://doi.org/10.1021/bi990356r>.
44. Meini MR, Llarrull LI, Vila AJ. 2015. Overcoming differences: the catalytic mechanism of metallo- β -lactamases. *FEBS Lett* 589:3419–3432. <https://doi.org/10.1016/j.febslet.2015.08.015>.
45. Brown NG, Horton LB, Huang W, Vongpunsawad S, Palzkill T. 2011. Analysis of the functional contributions of Asn233 in metallo- β -lactamase IMP-1. *Antimicrob Agents Chemother* 55:5696–5702. <https://doi.org/10.1128/AAC.00340-11>.
46. Christopheit T, Yang KW, Yang SK, Leiros HK. 2016. The structure of the metallo- β -lactamase VIM-2 in complex with a triazolylthioacetamide inhibitor. *Acta Crystallogr F Struct Biol Commun* 72:813–819. <https://doi.org/10.1107/S2053230X16016113>.
47. Meini MR, Tomatis PE, Weinreich DM, Vila AJ. 2015. Quantitative description of a protein fitness landscape based on molecular features. *Mol Biol Evol* 32:1774–1787. <https://doi.org/10.1093/molbev/msv059>.
48. LaCuran AE, Pegg KM, Liu EM, Bethel CR, Ai N, Welsh WJ, Bonomo RA, Oelschlaeger P. 2015. Elucidating the role of residue 67 in IMP-type metallo- β -lactamase evolution. *Antimicrob Agents Chemother* 59:7299–7307. <https://doi.org/10.1128/AAC.01651-15>.
49. Reference deleted.
50. Laraki N, Franceschini N, Rossolini GM, Santucci P, Meunier C, de Pauw E, Amicosante G, Frere JM, Galleni M. 1999. Biochemical characterization of the *Pseudomonas aeruginosa* 101/1477 metallo- β -lactamase IMP-1 produced by *Escherichia coli*. *Antimicrob Agents Chemother* 43:902–906.
51. Siemann S, Evanoff DP, Marrone L, Clarke AJ, Viswanatha T, Dmitrienko GI. 2002. N-Arylsulfonyl hydrazones as inhibitors of IMP-1 metallo- β -lactamase. *Antimicrob Agents Chemother* 46:2450–2457. <https://doi.org/10.1128/AAC.46.8.2450-2457.2002>.
52. Kabsch W. 2010. Xds. *Acta Crystallogr D Biol Crystallogr* 66:125–132. <https://doi.org/10.1107/S0907444909047337>.
53. Evans PR, Murshudov GN. 2013. How good are my data and what is the resolution? *Acta Crystallogr D Biol Crystallogr* 69:1204–1214. <https://doi.org/10.1107/S0907444913000061>.
54. Biasini M, Bienert S, Waterhouse A, Arnold K, Studer G, Schmidt T, Kiefer F, Gallo Cassarino T, Bertoni M, Bordoli L, Schwede T. 2014. SWISS-MODEL: evolutionary protein tertiary and quaternary structure using evolutionary information. *Nucleic Acids Res* 42:W252–W258. <https://doi.org/10.1093/nar/gku340>.
55. McCoy AJ, Grosse-Kunstleve RW, Adams PD, Winn MD, Storoni LC, Read RJ. 2007. Phaser crystallographic software. *J Appl Crystallogr* 40:658–674. <https://doi.org/10.1107/S0021889807021206>.
56. Adams PD, Afonine PV, Bunkoczi G, Chen VB, Davis IW, Echols N, Headd JJ, Hung LW, Kapral GJ, Grosse-Kunstleve RW, McCoy AJ, Moriarty NW,

- Oeffner R, Read RJ, Richardson DC, Richardson JS, Terwilliger TC, Zwart PH. 2010. PHENIX: a comprehensive Python-based system for macromolecular structure solution. *Acta Crystallogr D Biol Crystallogr* 66:213–221. <https://doi.org/10.1107/S0907444909052925>.
57. Emsley P, Cowtan K. 2004. Coot: model-building tools for molecular graphics. *Acta Crystallogr D Biol Crystallogr* 60:2126–2132. <https://doi.org/10.1107/S0907444904019158>.
58. Schrödinger, LLC. The PyMOL molecular graphics system, 1.8 ed. Schrödinger, LLC, New York, NY.
59. Christopeit T, Leiros HK. 2016. Fragment-based discovery of inhibitor scaffolds targeting the metallo- β -lactamases NDM-1 and VIM-2. *Bioorg Med Chem Lett* 26:1973–1977. <https://doi.org/10.1016/j.bmcl.2016.03.004>.
60. Kyte J, Doolittle RF. 1982. A simple method for displaying the hydrophobic character of a protein. *J Mol Biol* 157:105–132. [https://doi.org/10.1016/0022-2836\(82\)90515-0](https://doi.org/10.1016/0022-2836(82)90515-0).
61. Garau G, Garcia-Saez I, Bebrone C, Anne C, Mercuri P, Galleni M, Frere JM, Dideberg O. 2004. Update of the standard numbering scheme for class B β -lactamases. *Antimicrob Agents Chemother* 48:2347–2349. <https://doi.org/10.1128/AAC.48.7.2347-2349.2004>.